Clim Dyn (2012) 39:2219–2238
DOI 10.1007/s00382-012-1416-y

A tripolar pattern as an internal mode of the East Asian summer monsoon

Nagio Hirota · Masaaki Takahashi

Received: 25 July 2011 / Accepted: 31 May 2012 / Published online: 16 June 2012

Abstract A tripolar anomaly pattern with centers located around the Philippines, China/Japan, and East Siberia dominantly appears in climate variations of the East Asian summer monsoon. In this study, we extracted this pattern as the first mode of a singular value decomposition (SVD1) over East Asia. The squared covariance fraction of SVD1 was 59 %, indicating that this pattern can be considered a dominant pattern of climate variations. Moreover, the results of numerical experiments suggested that the structure is also a dominant pattern of linear responses, even if external forcing is distributed homogeneously over the Northern Hemisphere. Thus, the tripolar pattern can be considered an internal mode that is characterized by the internal atmospheric processes. In this pattern, the moist processes strengthen the circulation anomalies, the dynamical energy conversion supplies energy to the anomalies, and the Rossby waves propagate northward in the lower troposphere and southeastward in the upper troposphere. These processes are favorable for the pattern to have large amplitude and to influence a large area.

Keywords Monsoon · Climate variability · A linear model

1 Introduction

The East Asian summer monsoon (EASM) has complex and unique characteristics associated with the land–sea contrast of the Eurasian continent and the Pacific Ocean. Figure 1 shows a climatological field defined as an average during 1979–2005 in the June–July–August (JJA) seasons. Troughs are located around India, China, and Japan. An anticyclonic circulation is identified over the Pacific Ocean and East Siberia. Between the troughs and the Pacific High, geostrophic southwesterlies transport moisture to the midlatitudes forming a rainband called *baiu* in Japan and strong moisture gradients are zonally observed around 35°N. In the upper troposphere, a double jet structure exists over the Eurasian continent, which geostrophically balances with the temperature gradients of the midlatitudes and the coastline of the Arctic Sea.

The variations of the EASM have been discussed in many previous studies. For example, Wang et al. (2001) discussed the relationship between interannual variations of the EASM and El Nino Southern Oscillation during 1948–1997. They showed that atmospheric circulations around the Philippines in JJA seasons are significantly correlated with the sea surface temperature (SST) of the NINO3.4 region (170°–120°W, 5°S–5°N) in the precedent December–January–February (DJF) seasons. In other words, the Pacific High in the climatological field (see Fig. 1a) tends to extend farther southwestward during summer after El Nino compared to an average year. In addition to this high-pressure anomaly around the Philippines, there are also negative and positive pressure anomalies observed around China/Japan and East Siberia, respectively.

This tripolar climate anomaly pattern with centers located around the Philippines, China/Japan, and East Siberia (e.g. Fig. 2b, c) dominantly appears in climate variations of the EASM. Endo (2005) showed a spatial structure of interannual variabilities during 1958–2002 of JJA height fields associated with variations of the Indian

N. Hirota (✉) · M. Takahashi
Atmosphere and Ocean Research Institute,
The University of Tokyo, 5-1-5 Kashiwanoha,
Kashiwa, Chiba 277-8568, Japan
e-mail: nagio@aori.u-tokyo.ac.jp

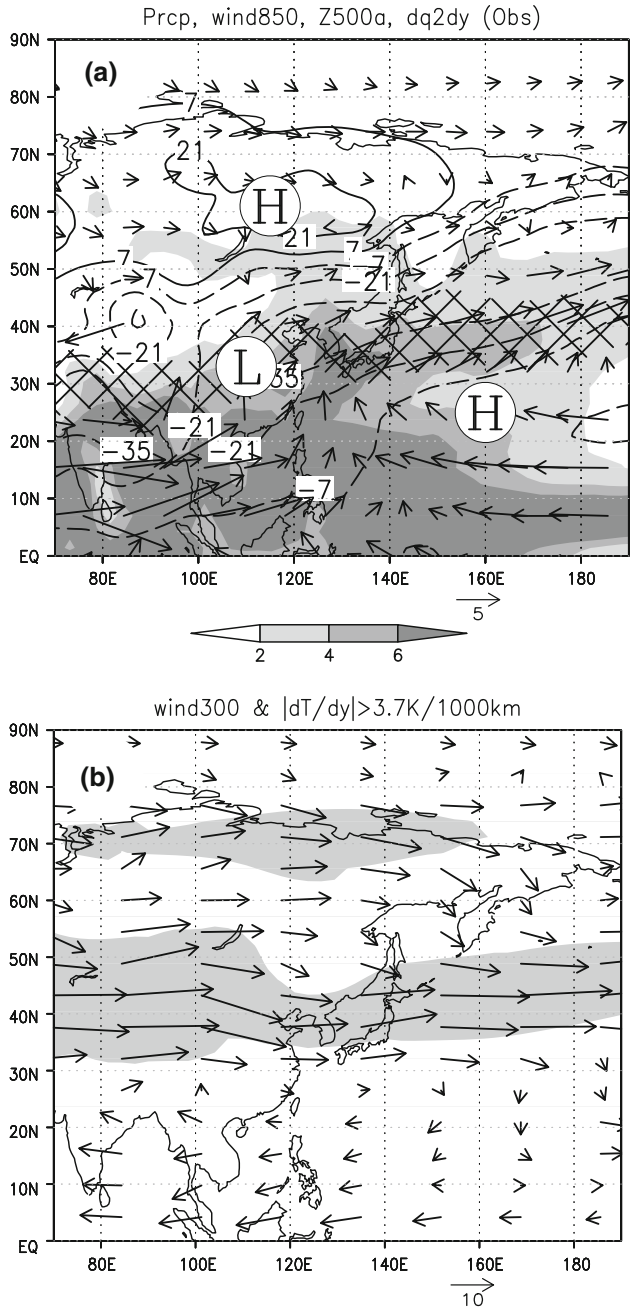

Fig. 1 A JJA climatological field. **a** Precipitation (*shadings*; mm day^{-1}), horizontal winds at 850 hPa (vectors; m s^{-1}), Z500 deviations from the zonal mean (*contours*; m), and 2m specific humidity gradients stronger than -4.5×10^{-9}kg kg^{-1}m^{-1} (*hatchings*). **b** Horizontal winds at 300 hPa (vectors; m) and meridional temperature gradients of the troposphere (1,000–300 hPa) stronger than −3.7 K (1,000 km)$^{-1}$ (*shadings*)

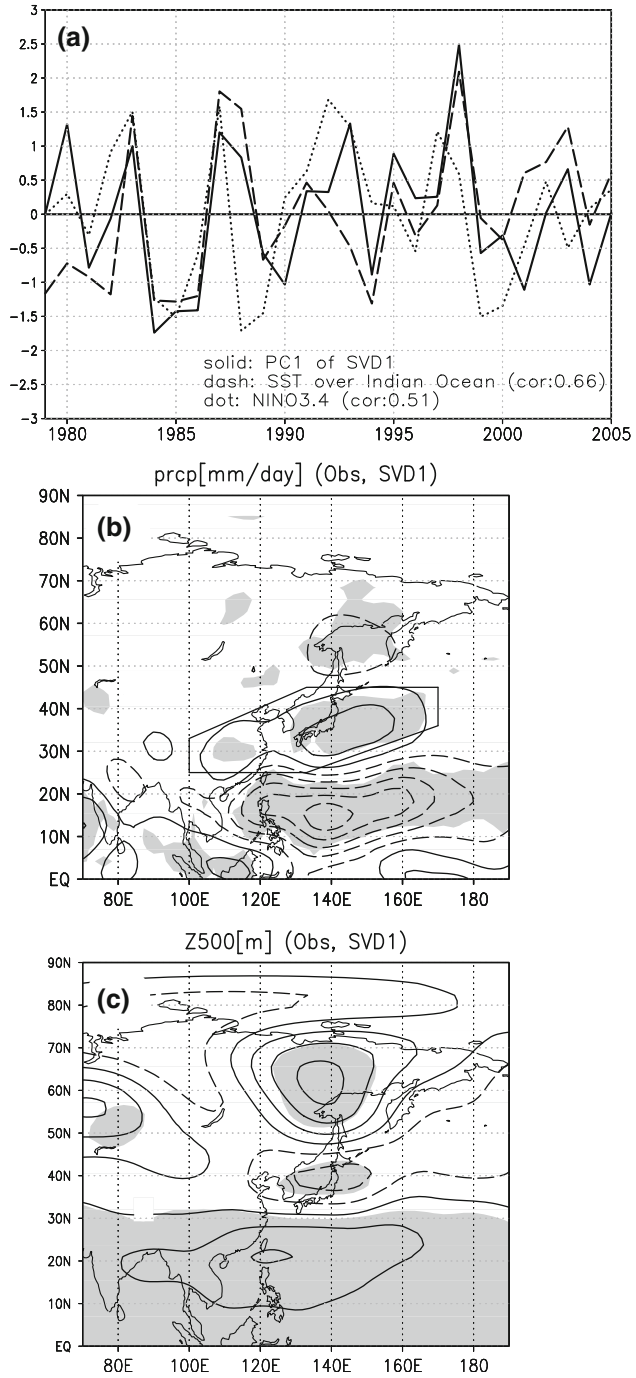

Fig. 2 **a** Time series of SVD1 over East Asia (*solid line*) in the JJA seasons, SST of the precedent MAM over the Indian Ocean (*dashed line*), and SST of the precedent DJF over the NINO3.4 region (*dotted line*) (normalized by standard deviations). The SVD analysis is applied to correlation matrix of JJA mean precipitation and Z500 during 1979–2005. Regression maps of **b** precipitation and **c** Z500 with respect to the SVD1. *Contours* are drawn with an interval of 0.4 (±0.2, ±0.6, ±1.0, …) mm day^{-1} in **b** and 4 (±2, ±6, ±10, …) m in **c**. *Shadings* in **b** and **c** denote significant anomalies at 95 % confidence level

Ocean SST (50°–120°E, 20°S–20°N) in the precedent March–April–May (MAM) seasons, which also had a tripolar structure. Hirota et al. (2005) showed linear trends of June precipitation during 1979–2003 having a tripolar structure. The climate response to doubled CO_2 concentrations in the climate model of Kimoto (2005) also suggested a tripolar pattern. Although these anomaly patterns are defined differently and are likely to be associated

with different types of external forcings, they have a similar tripolar structure.

The two anomalies around the Philippines and Japan are reminiscent of the Pacific–Japan (PJ) pattern, which is a dominant teleconnection pattern first identified by Nitta (1987). The pressure fields around Japan tend to be higher when convective activities around the Philippines are more active. Tsuyuki and Kurihara (1989) investigated this relationship using a linear barotropic model at a 300 hPa level and interpreted this pattern as Rossby waves excited by convective activities around the Philippines.

More recently, Kosaka and Nakamura (2010) suggested that the PJ pattern can be regarded as a dry dynamical mode. Besides the importance of the Rossby waves for the horizontal structure, they emphasized the role of dynamical energy conversion from the climatological mean field. In particular, they obtained a pattern similar to the observed PJ pattern as a second least-damped singular mode in a two-level dry model of a linearized quasi-geostrophic system. The singular mode in the model gains energy efficiently through barotropic energy conversion around the Philippines and baroclinic energy conversion around Japan. Similar energy conversions were also identified in observations (Fukutomi and Yasunari 1999, 2002; Yasutomi 2003; Kosaka and Nakamura 2006).

Previous researches on PJ patterns focused on the importance of the dry dynamical processes, but there are evidences suggesting that moist processes also play a role. The circulation anomalies of the PJ pattern accompany a large amount of precipitation (Kosaka and Nakamura 2006), and the associated diabatic heating contributes to the energy of the PJ pattern (Kosaka and Nakamura 2008). Lu and Lin (2009) suggested that heating associated with precipitation around China/Japan is important for upper topospheric circulations of the PJ pattern. In general, the impacts of diabatic heating associated with precipitation are thought to be large in the tropics where abundant moisture is available and relatively small in the higher latitudes. However, as described above, the monsoon southwesterlies at the lower troposphere transport a large amount of moisture to the midlatitudes in summer. Thus, this study investigates the role of moist processes in the midlatitudes around China/Japan as well as in the tropics around the Philippines.

Researchers have also been concerned with the high pressure anomaly over East Siberia in summer, as the associated northeasterlies, called Yamase, often bring a cool summer to Japan (Ninomiya and Mizuno 1985). Sato and Takahashi (2007) suggested that this anomaly again has characteristics of a dry dynamical mode. The linear barotropic model at the 300 hPa level showed that the pattern having a maximum over East Siberia is a dominant mode and explained that the mode obtains energy through barotropic energy conversion associated with the structure of the polar jet in the upper troposphere. Besides the dynamical energy conversion, Arai and Kimoto (2008) suggested that divergence of nonlinear vorticity flux also contributes to the formation of the pressure anomaly over East Siberia.

This study examines the physical reasons why the tripolar pattern appears so dominantly in EASM climate variations. As described above, this pattern is associated with various kinds of external factors for atmospheric variations, such as SST and CO_2 concentration. Therefore, this study expects that the basic structure of the pattern would be determined not by external factors, but by internal atmospheric processes, which probably function similarly in the different EASM variations. Although this study agrees that Rossby waves from the tropics are a very important concept for understanding the horizontal structure of the PJ pattern, it does not fully explain the tripolar structure. Considering Rossby waves as the balance of potential vorticity advection and effective beta, anomalies of the waves in a southwesterly basic state are likely to have a southwest–northeast orientation (cf. Nitta 1987; Tsuyuki and Kurihara 1989). However, the anomalies of the tripolar pattern are located almost in the same longitudes (south–north orientation). The relationship between the anomalies around Japan and East Siberia is also an interesting issue, which is not much discussed in previous researches. We also investigate how dynamical energy conversion and moist processes affect the structure and amplitude of the pattern.

This paper consists of the following sections: Sect. 2 describes the data used in the analyses; In Sect. 3, the tripolar structure is extracted as a dominant pattern; Sect. 4 discusses the internal processes associated with the pattern; In Sect. 5, numerical experiments are conducted to show processes important for the pattern; Sect. 6 is a summary and discussion.

2 Data

We analyzed the Japanese 25-year reanalysis and the JMA Climate Data Assimilation System (JRA25/JCDAS; Onogi et al. 2007) as well as CPC Merged Analysis of Precipitation (CMAP) estimated by rain gauge and satellite observations (Xie and Arkin 1997) during 1979–2005. The time intervals of the reanalysis and precipitation data were 6 h and 5 days, respectively. These data were analyzed on T42 ($\approx$2.8°) horizontal grids, which is the resolution of a numerical model used in Sect. 5.

We considered a climatological mean field, defined as a 27-year average of a 30-day running mean, as the basic state and discuss anomalies from this basic state (Wallace

and Gutzler 1981). Our study mainly focused on the interannual variability of the JJA average, except for "Appendix 1" where interseasonal variabilities and differences between June and August are discussed.

3 The tripolar pattern in reanalysis and observation data

To extract a dominant pattern of interannual variations, we performed a singular value decomposition (SVD) to a correlation matrix of the JJA mean precipitation and the 500 hPa geopotential height (Z500) over East Asia (70°E–170°W, 0°–90°N) during 1979–2005. Note that the correlation matrix is weighted with area of each grid box. A solid line in Fig. 2a showed the time series of the first mode (SVD1) for precipitation, which is strongly related to that of Z500 with a correlation coefficient of 0.92. The regression maps of precipitation and Z500 with respect to the time series for precipitation were shown in Fig. 2b, c. Anomalies were identified around the Philippines (100°E–170°W, 5°–25°N), China/Japan (100°E–170°W, 25°–45°N), and East Siberia (110°E–170°W, 45°–80°N) in both the precipitation and Z500 anomaly fields. The squared covariance fraction (SCF) of SVD1 was 59 %, and SVD1 was clearly separated from higher modes (North et al. 1982).

As shown in the previous studies (Wang et al. 2001; Endo 2005), the time series (solid line, Fig. 2a) in the JJA seasons showed a statistically significant relationship with the SST of the precedent MAM over the Indian Ocean (50°–120°E, 20°S–20°N; dashed line; correlation coefficient is 0.66) and the SST of the precedent DJF over the NINO3.4 region (170°–120°W, 5°S–5°N; dotted line; correlation coefficient is 0.51). Moreover, the correlation coefficient between the time series and precipitation around Japan (black box indicated in Fig. 2b) is 0.77, suggesting its importance for the interannual variations of the rainband in the midlatitudes (see Fig. 1a).

Similar patterns can be obtained in many other ways as well. For example, Fig. 3 shows an empirical orthogonal function (EOF) analysis of a correlation matrix of the JJA mean Z500 over the Northern Hemisphere. The first mode that contributes to 37 % of the total correlations has a tripolar structure over East Asia. Statistically significant anomalies are identified over the entire tropics, Central Asia, North America, and East Asia. Of these anomalies, the tripolar structure over East Asia is the most prominent feature, as this pattern appears to be a dominant pattern mainly over East Asia and may be related to other parts of the Northern Hemisphere as well. This result reinforces the robustness of the structure and its importance as a dominant climate variability pattern of EASM. The robustness

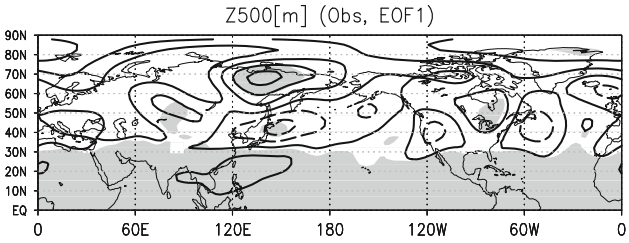

Fig. 3 Same as Fig. 2c, but regression maps with respect to the EOF1 of JJA mean Z500 over the Northern Hemisphere

of the pattern is further supported by SVD analyses for June average data, August average data, and daily average data in "Appendix 1".

Since SVD and EOF analyses may yield a statistical artifact, the pattern can be an artificial combination of a tropical-midlatitude dipole pattern and a midlatitude-East Siberian dipole pattern having a common signal around China/Japan. To support the connections between southernmost and northernmost anomalies, we made correlation maps of Z500 with respect to precipitation averaged in a box near the Philippines (110°E–120°E, 10°–20°N) and the Sea of Othotsk (140°E–150°E, 50°–60°N) as shown in Fig.4. The both correlation maps show the tripolar structure similar to that obtained from SVD and EOF analyses.

4 Internal processes associated with the pattern

In this section, we describe a moisture budget, a heat budget, a vorticity budget, and a dynamical energy analysis in the tripolar anomaly field, which is defined as regressions to the SVD1 of the JJA mean precipitation and Z500 over East Asia (Fig. 2). Then, we discuss how the internal processes such as moist processes, energy conversion, and Rossby waves affect and determine the structure and amplitude of the pattern.

We use linearized primitive equations in the following analyses. The primitive equations of anomalous variables $(\,)'$ linearized about the climatological mean field $\overline{(\,)}$ in the pressure coordinate system (longitude λ, latitude φ, and pressure p) are

$$\begin{aligned}\frac{\partial \boldsymbol{u}'}{\partial t} = &-\left(\overline{\boldsymbol{u}}\cdot\nabla+\bar{\omega}\frac{\partial}{\partial p}\right)\boldsymbol{u}'-\frac{\bar{u}\tan\varphi}{R}(-v',u')\\ &-\left(\boldsymbol{u}'\cdot\nabla+\omega'\frac{\partial}{\partial p}\right)\overline{\boldsymbol{u}}-\frac{u'\tan\varphi}{R}(-\bar{v},\bar{u})\\ &-f(-v',u')-\nabla\Phi'+\mathcal{N}_{\boldsymbol{u}} \qquad (1)\end{aligned}$$

$$\begin{aligned}\frac{\partial T'}{\partial t} = &-\overline{\boldsymbol{u}}\cdot\nabla T'-\boldsymbol{u}'\cdot\nabla\bar{T}+\left(\frac{R_dT'}{pC_p}-\frac{\partial T'}{\partial p}\right)\bar{\omega}+S_p\omega'\\ &+\mathcal{N}_T+Q' \qquad (2)\end{aligned}$$

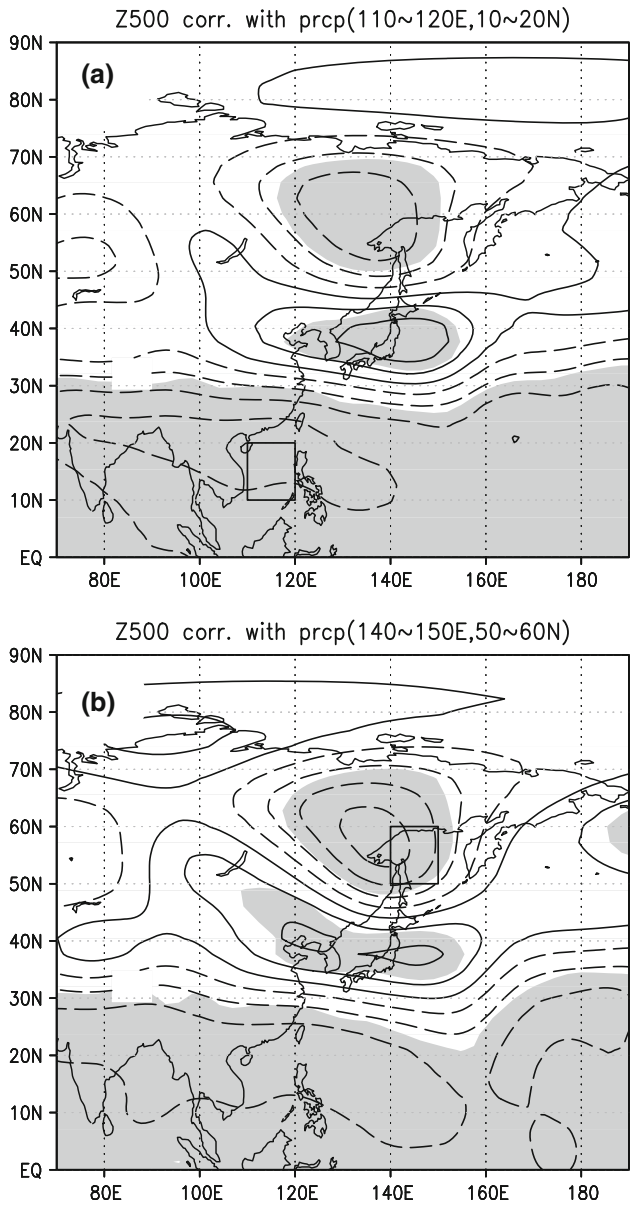

Fig. 4 Z500 correlation maps with respect to precipitation near **a** the Philippines (110°E–120°E, 10°–20°N) and **b** the Sea of Othotsk (140°E–150°E, 50°–60°N). *Contours* are drawn with an interval of 0.2 ($\pm 0.1, \pm 0.3, \pm 0.5, \ldots$)

$$\frac{\partial q'}{\partial t} = -\nabla \cdot (\overline{\boldsymbol{u}} q') - \frac{\partial (\bar{\omega} q')}{\partial p} - \nabla \cdot (\boldsymbol{u}' \bar{q}) - \frac{\partial (\omega' \bar{q})}{\partial p} + \mathcal{N}_q + S' \tag{3}$$

where Q' is diabatic heating, S' is moisture sink (or source), $\mathcal{N}$ represents nonliner effects, $S_p \left(\equiv \frac{R_d \bar{T}}{p C_p} - \frac{\partial \bar{T}}{\partial p} \right)$ is a static stability parameter, and other notations are standard. The nonlinear effects $\mathcal{N}$ are associated with high frequency disturbances with a period shorter than 3 months. An example of $\mathcal{N}$ is $-(\boldsymbol{u}_a \cdot \nabla \boldsymbol{u}_a)'$, where $(\,)_a$ shows a deviation of 6 hourly data from the climatological mean field, which is defined as a 27-year average of a 30-day running mean. Note that the nonlinear effects of the disturbances with a period shorter than 6 h are not considered in these analyses because the time interval of the data is 6 h.

The tendency terms on the left-hand side of Eqs. (1–3) are very small in 3 month averages, so they are neglected in the following budget analyses.

4.1 A moisture budget analysis

To derive an equation for a moisture budget, we integrate Eq. (3) from the surface ($p = p_s$) to the top of the atmosphere ($p = 0$) and use $\int_{p_s}^{0} S \frac{dp}{g} = -$precipitation $+$ evaporation. Thus,

$$\text{Precipitation}' \approx -\int_{p_s}^{0} \nabla \cdot (\overline{\boldsymbol{u}} q') \frac{dp}{g} - \int_{p_s}^{0} \nabla \cdot (\boldsymbol{u}' \bar{q}) \frac{dp}{g} + \int_{p_s}^{0} \mathcal{N}_q \frac{dp}{g} + \text{evapolation}'. \tag{4}$$

This equation shows that the precipitation anomalies correspond to moisture convergence associated with specific humidity anomalies, moisture convergence associated with circulation anomalies, a nonlinear term, and evaporation anomalies. This approximation is valid because the time scales of cloud processes are sufficiently shorter than 3 months.

The precipitation anomalies (Fig. 2b) mostly correspond to the moisture convergence due to the circulation anomalies [the second term on the right-hand side of Eq. (4)] shown in Fig. 5, and the other terms are very small (figures are not shown). Because moisture is concentrated in the lower troposphere, the circulation anomalies in the lower levels are mainly responsible for this convergence. Vectors in Fig. 5 show the moisture flux due to the circulation anomalies. The northeastward moisture flux to China/Japan corresponds to the anomalous moisture transport by the stronger monsoon southwesterlies in the lower troposphere.

4.2 A heat budget analysis

A heat budget of Eq. (2) for the tripolar anomaly field is shown in Fig. 6. We calculate horizontal advection [the first and second terms on the right-hand side of the thermodynamic equation (2)], adiabatic heating (the third and fourth terms), a nonlinear term (the fifth term), and a diabatic heating (the sixth term). The dominant terms around the Philippines and China/Japan are the adiabatic heating and the diabatic heating, which balance each other. In addition to these two terms, horizontal advection and a nonlinear term also have some contribution in the higher

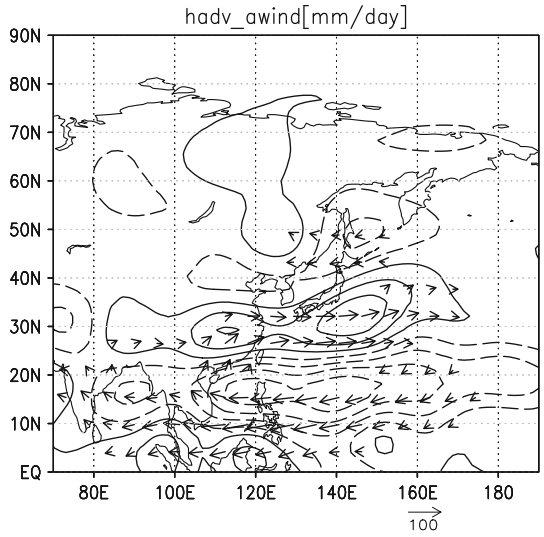

Fig. 5 Moisture flux associated with anomalous circulations $\int_{p_s}^{0} \boldsymbol{u}'\bar{q}\frac{dp}{g}$ (vectors; kg m^{-1} s^{-1}) and its convergence $-\int_{p_s}^{0} \nabla\cdot(\boldsymbol{u}'\bar{q})\frac{dp}{g}$ (*contours*). *Contours* are drawn with an interval of 0.4 ($\pm 0.2, \pm 0.6, \pm 1.0, \ldots$) mm day^{-1}

latitudes. Cooling by the horizontal advection over the Sea of Okhotsk (150°E, 55°N) is more conspicuous in the lower troposphere, which is consistent with the result of Ninomiya and Mizuno (1985).

The diabatic heating Q' is estimated as a residual of the thermodynamic equation (Yanai et al. 1973). Note that the nonlinear $\mathcal{N}_T$ associated with high frequency disturbances is not included in this Q' for clearer interpretation of each term. Because the horizontal pattern of the diabatic heating (Fig. 6d) is similar to the precipitation anomaly pattern (Fig. 2b), a large part of the diabatic heating is possibly the condensation heating of the precipitation anomalies. To quantitatively support this idea, we compared the vertical integral of the diabatic heating $\frac{C_p}{L}\int_{p_s}^{0} Q'\frac{dp}{g}$ (figures are not shown) with the precipitation anomalies. Both have a minimum of about -2 mm day^{-1} around the Philippines and a maximum of about 1 mm day^{-1} around Japan, and their horizontal patterns are very similar to each other. Therefore, the diabatic heating associated with the tripolar pattern is mostly the condensation heating around the Philippines and China/Japan.

4.3 A vorticity budget analysis

A vorticity equation is derived by calculating the rotation of the momentum equation (1). We applied the quasi-geostrophic approximation and used the omega equation to investigate the effects of diabatic heating in the budget, which is closely related to the moist processes. The vorticity equation is

$$0 \approx -\overline{\boldsymbol{u}}_\psi\cdot\nabla\xi' - \boldsymbol{u}'_\psi\cdot\nabla(f+\bar{\xi}) + f_0\frac{\partial\omega'_D}{\partial p} + f_0\frac{\partial\omega'_Q}{\partial p} + \mathcal{N}_\xi \tag{5}$$

where f_0 is the Coriolis parameter at 45°N, ξ is relative vorticity, $\psi \equiv \Phi/f_0$ is stream function, $\boldsymbol{u}_\psi \equiv \left(-\frac{\partial\psi}{\partial y}, \frac{\partial\psi}{\partial x}\right)$ is the geostrophic components of the horizontal wind, and

$$\omega' = \omega'_D + \omega'_Q \tag{6}$$

$$\begin{aligned}\omega'_D \equiv & \left(\nabla^2 + \frac{f_0^2 p}{S_p R_d}\frac{\partial^2}{\partial p^2}\right)^{-1} \\ & \times\left[-\frac{f_0 p}{S_p R_d}\frac{\partial}{\partial p}\{-\overline{\boldsymbol{u}}_\psi\cdot\nabla\xi' - \boldsymbol{u}'_\psi\cdot\nabla(\bar{\xi}+f_0)\}\right] \\ & + \left(\nabla^2 + \frac{f_0^2 p}{S_p R_d}\frac{\partial^2}{\partial p^2}\right)^{-1} \\ & \times\left[-\frac{f_0 p}{S_p R_d}\nabla^2\left(\overline{\boldsymbol{u}}_\psi\cdot\nabla\frac{\partial\psi'}{\partial p} + \boldsymbol{u}'_\psi\cdot\frac{\partial\bar{\psi}}{\partial p}\right)\right]\end{aligned} \tag{7}$$

$$\omega'_Q \equiv \left(\nabla^2 + \frac{f_0^2 p}{S_p R_d}\frac{\partial^2}{\partial p^2}\right)^{-1}\left[-\frac{p}{S_p R_d}\nabla^2\left(\frac{R_d}{p}Q'\right)\right]. \tag{8}$$

Equations (6–8) constitute a linearized omega equation. The third term of Eq. (5) is a stretching term associated with vorticity and temperature advection, and the fourth term is a stretching term associated with diabatic heating. Note that the validity of the quasi-geostrophic approximation is confirmed by comparing the results in the primitive system.

The vorticity anomalies and each term of Eq. (5) at 850 and 300 hPa are shown in Figs. 7 and 8, respectively. Wave activity flux (WAF), which is parallel to the group velocity of Rossby waves (Takaya and Nakamura 2001), is also shown in Figs. 7a and 8a.

In the lower troposphere at 850 hPa, negative–positive–negative vorticity anomalies from the Philippines to East Siberia are identified corresponding to the precipitation and Z500 anomalies. The northward WAF from the Philippines and the balance of horizontal advection, effective beta, and a dynamical stretching term $f_0\frac{\partial\omega'_D}{\partial p}$ suggest that the anomalies around the Philippines and China/Japan can be interpreted as baroclinic Rossby waves. In addition to the dynamical balance, the stretching term associated with diabatic heating $f_0\frac{\partial\omega'_Q}{\partial p}$ also shows a large contribution suggesting the importance of the moist processes. The dominant term over the Sea of Okhotsk is $f_0\frac{\partial\omega'_D}{\partial p}$, and is associated with downward motions ($\omega_D{}' > 0$). Further decomposition of $f_0\frac{\partial\omega'_D}{\partial p}$ using the Eq. (7) revealed that both vorticity and temperature advection contribute to the downward motions (figures are not shown). For example,

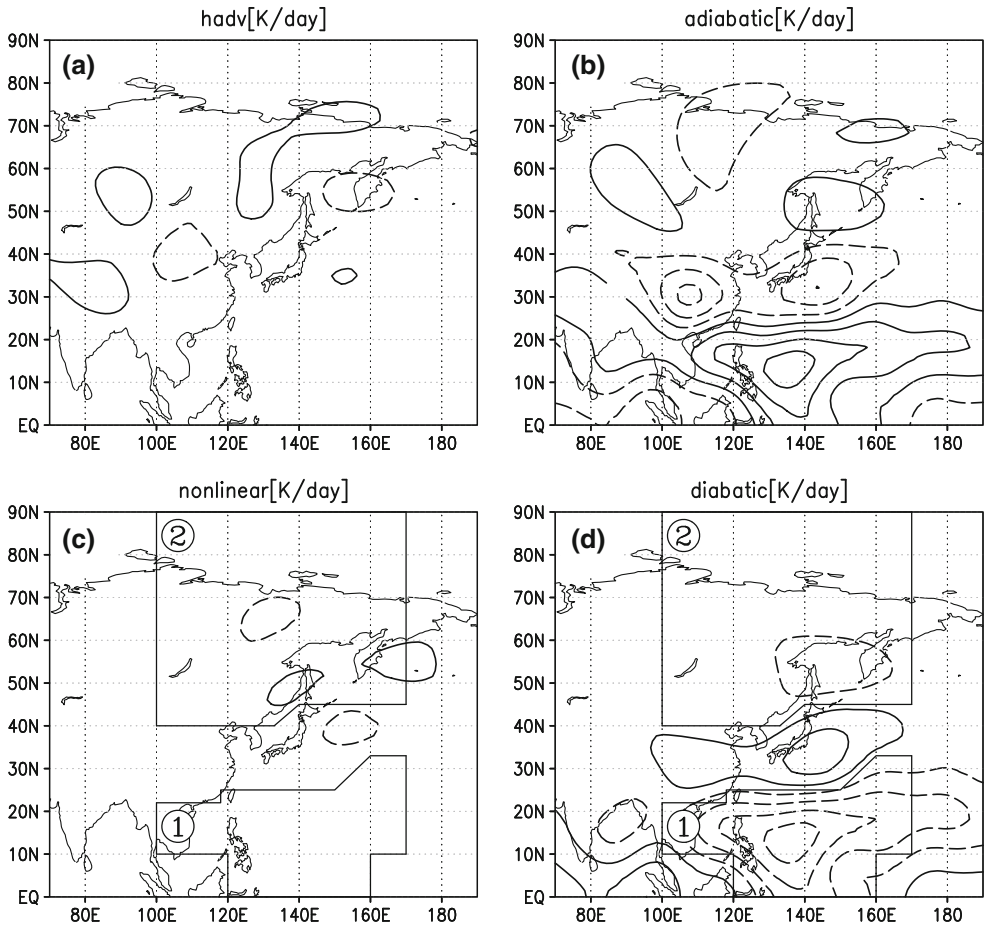

Fig. 6 A heat budget of the anomaly field at 500 hPa. **a** Horizontal advection $-\overline{\boldsymbol{u}} \cdot \nabla T' - \boldsymbol{u}' \cdot \nabla \bar{T}$, **b** adiabatic heating $\left(\frac{R_d T'}{p C_p} - \frac{\partial T'}{\partial p}\right)\bar{\omega} + S_p \omega'$, **c** a nonlinear term $\mathcal{N}_T$, and **d** diabatic heating Q'. *Contours* are drawn with an interval of 0.2 $(\pm 0.1, \pm 0.3, \pm 0.5, \ldots)$ K day^{-1}

the positive vorticity anomaly around Japan is advected northeastward to the Sea of Okhotsk by the climatological southwesterlies in the lower troposphere (Figs. 1a, 7b), whereas the negative vorticity anomaly around East Siberia is advected southeastward in the upper troposphere (Figs. 1b, 8b). Therefore, the positive advection in the lower troposphere and the negative advection in the upper troposphere results in the downward motion $\omega_D \sim -\frac{\partial}{\partial p}(-\overline{\boldsymbol{u}} \cdot \nabla \xi') > 0$. The anomalous descent (Figs. 7d, 8d) is collocated with upper-tropospheric anticyclonic advection anomaly (Fig. 8b), whereas lower-tropospheric advection (Fig. 7b) is shifted eastward from the descent. This result suggests a dominant role of upper-tropospheric advection on the descent. The stretching term associated with diabatic heating $f_0 \frac{\partial \omega'_Q}{\partial p}$ also shows some contribution to the anticyclonic vorticity at 850 hPa over the Sea of Okhotsk.

In the upper troposphere at 300 hPa, negative–positive–negative vorticity anomalies are located in East Siberia to the south of Japan, and the WAF directs southeastward from East Siberia (Fig. 8a). The dominant terms around East Siberia and Japan are horizontal advection and effective beta, which form the balance of barotropic Rossby waves, and the two stretching terms are relatively small. Nonlinear term $\mathcal{N}_\xi$ also has a large value.

4.4 Dynamical energy conversion from the climatological mean field

In our investigation of energy exchange between the anomaly and climatological fields associated with the tripolar pattern, we defined the total energy of the anomalies as $\left(\frac{u'^2+v'^2}{2} + \frac{R_d T'^2}{2 S_p p}\right)$. Dynamical energy conversion of the anomalies from the climatological field is expressed as

$$-\boldsymbol{u}' \cdot \left(\boldsymbol{u}' \cdot \nabla + \omega' \frac{\partial}{\partial p}\right)\overline{\boldsymbol{u}} - \frac{R_d T'}{S_p p} \boldsymbol{u}' \cdot \nabla \bar{T}. \tag{9}$$

The first term in Eq. (9) represents the barotropic energy conversion (Simmons et al. 1983) and the second term represents the baroclinic energy conversion. Figure 9 shows the total dynamical energy conversion of Eq. (9)

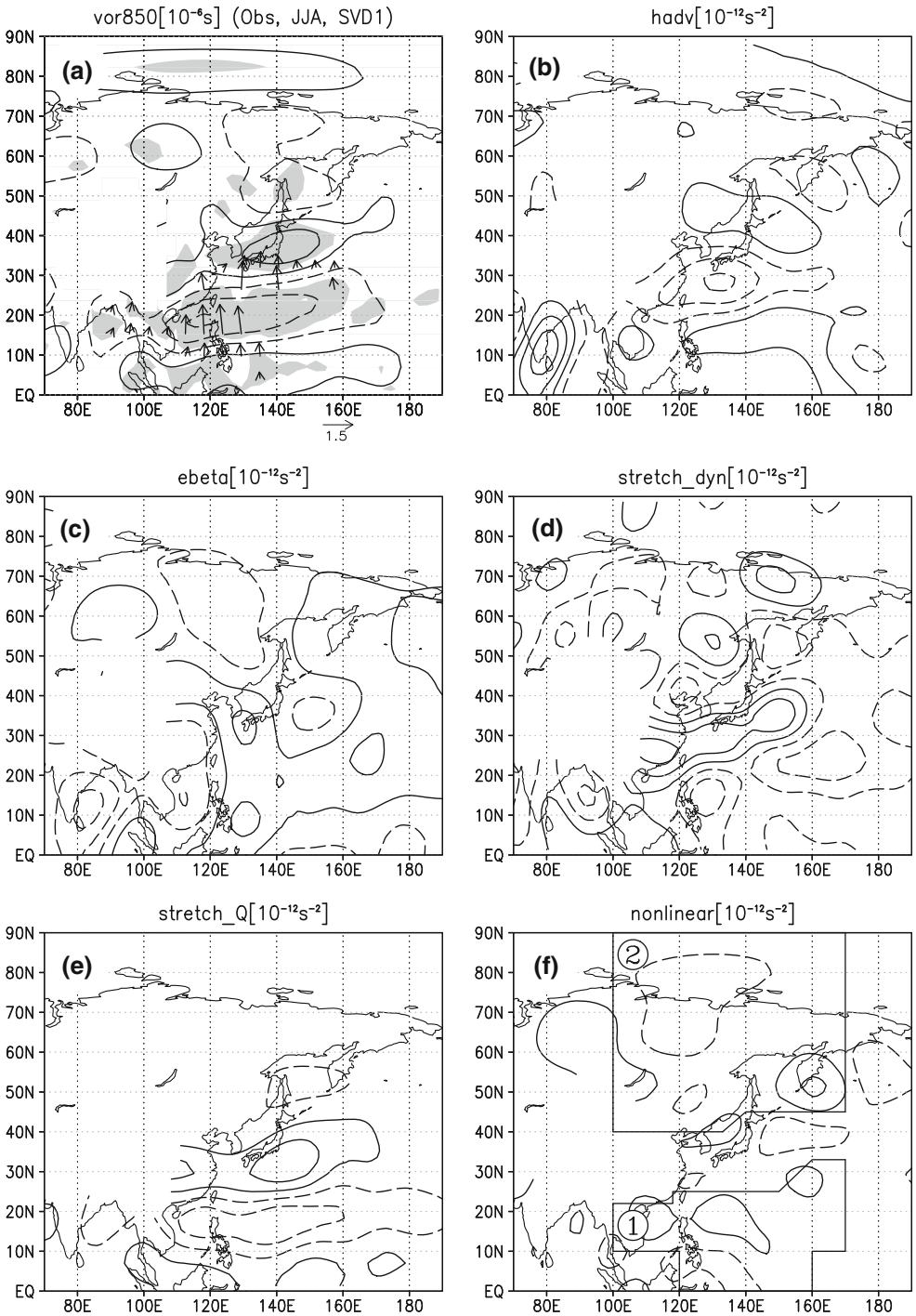

Fig. 7 **a** Vorticity anomalies (*contours*) and WAF (vectors; m^2s^{-2}) at 850 hPa, and *shadings* denotes significant anomalies at 95 % confidence level. A vorticity budget of the anomaly field at 850 hPa. **b** Horizontal advection associated with climatological circulations $-\overline{\boldsymbol{u}}_\psi \cdot \nabla\xi'$, **c** effective beta $-\boldsymbol{u}'_\psi \cdot \nabla(f+\overline{\xi})$, **d** a stretching term associated with horizontal vorticity and temperature advection $f_0\frac{\partial\omega'_p}{\partial p}$, **e** a stretching term associated with diabatic heating $f_0\frac{\partial\omega'_Q}{\partial p}$, and **f** a nonlinear term $\mathcal{N}_\xi$. *Contours* are drawn with an interval of 12 $(\pm 6, \pm 18, \pm 30, \ldots) \times 10^{-6}$ s^{-1} in **a** and 4 $(\pm 2, \pm 6, \pm 10, \ldots) \times 10^{-12}$ s^{-2} in **b–f**

averaged from 1,000 to 300 hPa. The positive energy conversion around the Philippines (120°E, 10°N), East Siberia (125°E, 70°N), Japan (130°E, 40°N), and northeast of Japan (160°E, 55°N) represents the energy supply to the anomalies from the climatological field. Note that negative values of energy conversion are also identified especially over the higher latitudes. They are associated with phases of the anomalies and partially compensate the positive energy conversion described above. Still, an average of the energy conversion over a large domain (70°E–170°W, 45°N–80°N) is largely positive, so the energy conversion contribute to the energy of the anomaly pattern.

4.5 Discussion about how the dominant tripolar pattern is determined

In this subsection, we discuss how the tripolar pattern is determined and why the pattern is dominant. Figure 10

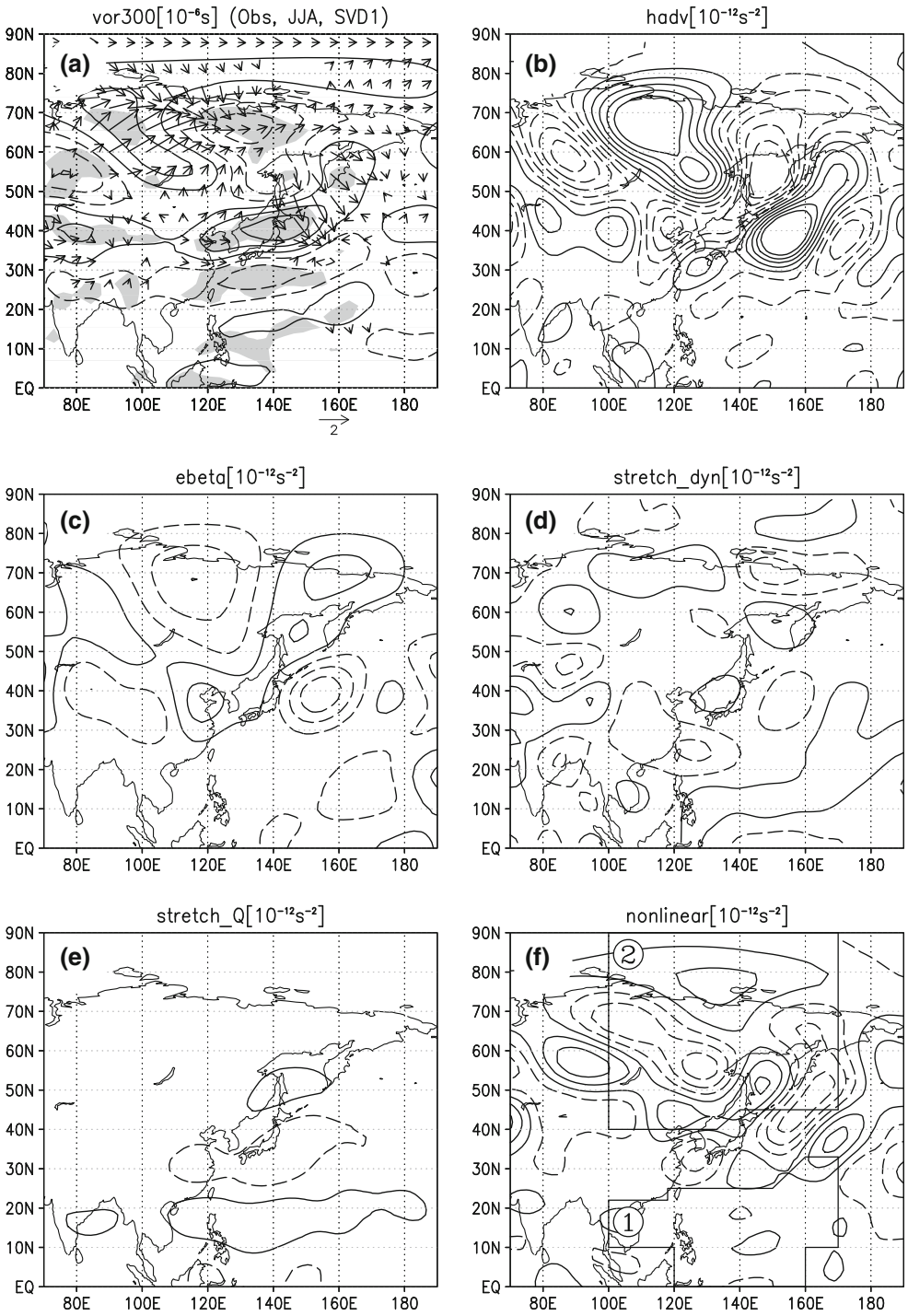

Fig. 8 Same as Fig. 7, but at 300 hPa. *Contours* are drawn with an interval of 16 $(\pm 8, \pm 24, \pm 30, \ldots) \times 10^{-6}$ s^{-1} in **a** and 8 $(\pm 4, \pm 12, \pm 20, \ldots) \times 10^{-12}$ s^{-2} in **b–f**

summarizes internal processes involved in the pattern. Ideas discussed here will further be examined in the next section using a numerical model.

The results of the moisture, heat, and lower-level vorticity budget suggest following processes. The anticyclonic circulation around the Philippines accompanies southwesterlies to China/Japan in the lower levels. The stronger monsoon southwesterlies converge moisture around China/Japan. The diabatic heating of the precipitation anomalies thermodynamically balances with the adiabatic heating of the vertical motions, and the air column stretching by the vertical motions contributes to the cyclonic circulation anomaly. These processes can cause the anomalies around the Philippines and China/Japan to have large amplitude with the opposite signs to each other. These strong interactions of circulations and precipitation are reasonable over

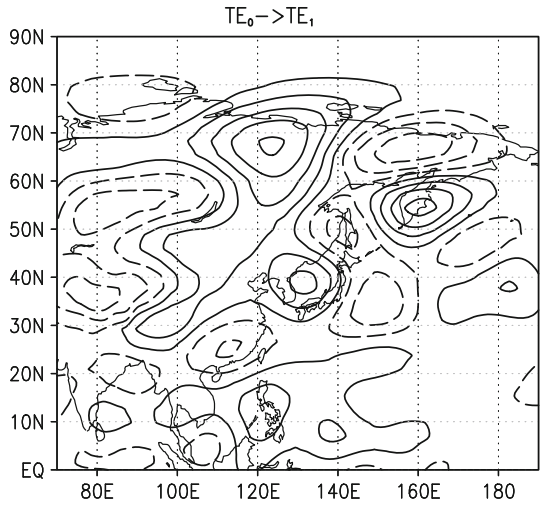

Fig. 9 Energy conversion (*contours*) averaged from 1,000 to 300 hPa. *Contours* are drawn with an interval of 1 $(\pm 0.5, \pm 1.5, \pm 2.5, \ldots) \times 10^{-6}$ J kg^{-1} s^{-1}

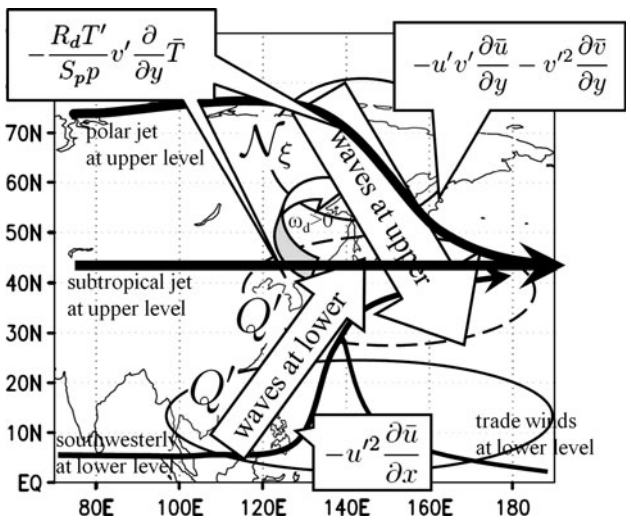

Fig. 10 A schematic figure of the internal processes involved in the tripolar pattern (*three ovals*). *Thin* and *thick solid arrows* indicate horizontal winds in the *lower* and *upper* troposphere, respectively. Q' is diabatic heating, $\mathcal{N}_\xi$ is nonlinear vorticity divergence, *three boxes* with an equation indicate dynamical energy conversion, *box arrows* show Rossby waves, and a semicircular arrow between Japan and East Siberia shows dynamically induced downward motions

the low and midlatitudes of East Asia as abundant moisture $\bar{q}$ is available owing to the monsoon circulations. However, we cannot say that the midlatitude convergence is a cause of precipitation from these diagnostic analyses because convergence is also a response to precipitation. A triggering of precipitation anomalies by remotely-induced anomalous convergence is supported by model results presented in Sect. 2.

The analysis of the omega equation in Sect. 3 suggests that the effects from the south reach farther to the north of Japan. For example, when the vorticity anomaly in the lower troposphere over Japan is positive, the advection of the vorticity anomaly by the climatological southwesterlies balances with the downward motions, which corresponds to the negative stretching term $f_0 \frac{\partial \omega'_p}{\partial p}$ over the Sea of Othotsk.

The nonlinear term $\mathcal{N}_\xi$ also have large values in the mid and highlatitudes, of which importance is noted by Hirota et al. (2005) and Arai and Kimoto (2008). This nonlinear term is mostly convergence of horizontal vorticity flux associated with high frequency disturbances $-\nabla \cdot (\boldsymbol{u}_a \xi_a)'$. The effects of this nonlinear term will be examined in Sect. 5.

As described in Sect. 4, the large energy supplies to the anomaly field through the dynamical energy conversion are identified near the three anomalies. The most prominent energy conversion is located around East Siberia, which is mostly due to $\left(-\frac{v'T'}{S}\frac{\partial \bar{T}}{\partial y}\right)$ and is associated with the baroclinicity of the climatological field between the Eurasian continent and the Arctic Sea. This suggests the importance of the processes at highlatitudes for the tripolar pattern in contrast with the PJ pattern, in which the processes in low and midlatitudes are emphasized.

The other energy conversions are also related to the structure of the climatological field. The energy conversion around the Philippines mostly stems from barotropic energy conversion $\left(-u'^2 \frac{\partial \bar{u}}{\partial x}\right)$ corresponding to the large gradient $\left|\frac{\partial \bar{u}}{\partial x}\right|$ associated with the monsoon westerlies from the Indian Ocean and the trade winds over the Pacific in the lower troposphere (Fig. 1a; Yasutomi 2003; Kosaka and Nakamura 2006). The conversion around Japan $\left(-\frac{v'T'}{S}\frac{\partial \bar{T}}{\partial y}\right)$ is found where the large temperature gradient of the subtropical jet exists (Fig. 1b), whereas that over northeast of Japan $\left(-u'v'\frac{\partial \bar{u}}{\partial y} - v'^2 \frac{\partial \bar{v}}{\partial y}\right)$ is related to the wind velocity gradient associated with the horizontal structure of the subpolar jet. These interactions with the climatological field are likely to be one of the factors that determine the location of the three anomalies. Note that the location of energy supplies and anomalies are not necessarily at the same place because disturbances may be advected and propagated as follows.

The concept of Rossby waves is useful to explain the relationships among the three anomalies. Similar to the PJ pattern, the anomalies around the Philippines and Japan can be interpreted as Rossby waves propagating northward at the lower troposphere. In contrast, the Rossby waves in the upper troposphere propagate southeastward from East Siberia, which again support the importance of the processes at high latitudes. It is interesting that the Rossby waves from the south and north somewhat influence the

midlatitudes of East Asia. These coupled waves are closely related to the climatological structure of the southwesterlies in the lower levels and the northwesterlies in the upper levels. The commitments of the two waves explain the south–north orientation of the three anomalies rather than the southwest–northeast orientation in simple Rossby waves of the PJ pattern (cf. Nitta 1987; Tsuyuki and Kurihara 1989).

The propagation of the Rossby waves can also be identified in time evolutions of the pattern shown in Fig. 11. To obtain the time evolutions, we first calculated a daily time series of the SVD1 defined as pattern correlations between daily precipitation anomaly from the climatological mean field and the precipitation pattern of the SVD1 shown in Fig. 2b. Then lag regressions of Z500 with respect to the daily time series and associated WAF are calculated.

On the −15th day, the WAF is identified only over Central Siberia. On the −10th day, the WAF extends eastward as the Z500 anomaly over East Siberia develops, and the small northward WAF appears around the Philippines. From the −5th day to the 0 day, the WAF grows larger and the tripolar structure is obtained, which are similar to that shown in Figs. 2c, 7a, and 8a. Note that the northward WAF around the Philippines is located only in the lower troposphere, whereas the southeastward WAF from East Siberia is concentrated mostly in the upper troposphere.

Thus, the moist processes, the dynamical energy conversion, and the Rossby wave couplings associated with the characteristics of the climatological field are all interrelated, and these complex internal processes determine the horizontal tripolar structure. Moreover, the positive feedbacks of the moist processes and the dynamical energy conversion strengthen and maintain the amplitude of each anomaly. These processes are favorable for the tripolar pattern to be the dominant pattern of the climate variabilities over East Asia.

5 Experiments using a linear primitive model

In this section, ideas suggested in the previous section are investigated using a numerical model. We newly developed

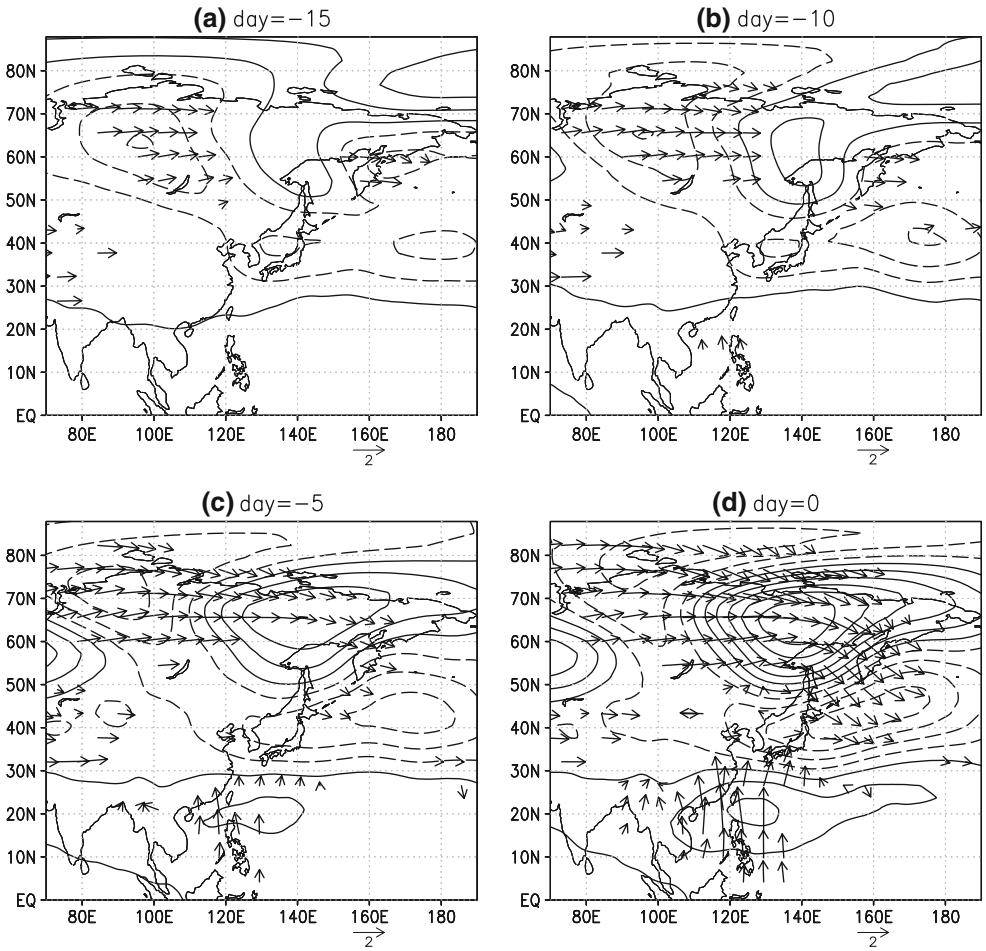

Fig. 11 Lag regressions of Z500 (*contours*) with respect to the daily time series of the SVD1 (see text for details) and associated WAF (vectors; $m^2\ s^{-2}$) averaged from 850 to 300 hPa. **a** The −15th day, **b** the −10th day, **c** the −5th day, and **d** the 0 day. *Contours* are drawn with an interval of 4 $(\pm 2, \pm 6, \pm 10, \ldots)$ m

a linear primitive model based on Numaguchi et al. (1995), Watanabe and Kimoto (2000 2001), and Satoh (2004). The governing equations of the model are the primitive equations linearized about the basic state in the σ ($\equiv$pressure/surface pressure) coordinates. The horizontal resolution of the model was T42 ($\approx$2.8°) and the model has 20 levels. Rayleigh friction, Newtonian cooling, and ∇^4 horizontal diffusion are included. The e-folding time of friction and cooling is set to 3 days for $0.995 < \sigma \leq 0.9$, 30 days for $0.9 < \sigma \leq 0.025$, and 1 day for $0.025 < \sigma \leq 0.0083$ (Branstator 1990; Watanabe and Jin 2003). The strong friction at the boundary layers mimics a turbulent mixing process. Because of the strong friction at the bottom and top of the model, baroclinic instability activities are limited in this model, which are not the interest of this study. The e-folding time of horizontal diffusion is set to 0.5 day for the largest wave number. The linear model consists of dry and moist versions. The moist processes are based on Watanabe and Jin (2003). When circulation anomalies produce convective instability (convective available potential energy >0 J kg^{-1}), temperature and moisture profiles are adjusted to moist adiabat with a time scale of 2 h.

This model calculates a linear response to prescribed forcings of diabatic heating [Q' in the Eq. (2)], moisture sink [S' in the Eq. (3)], and nonlinear terms ($\mathcal{N}$ in the Eqs. (1–3). As described in Sect. 4, diabatic heating Q' and moisture sink S' are mainly due to convective activities, whereas the nonlinear terms $\mathcal{N}$ are associated with disturbances with a period shorter than 3 months. The linear model is integrated for 20 days, with prescribed forcings imposed at each time step. The model response reached almost steady state on the 15th day. Thus, we discuss an average of days 15–20 as a steady response to the forcings (Enomoto et al. 2003).

To examine the model performance, we first conducted an experiment calculating a linear response to Q', S', and $\mathcal{N}$ over the entire globe at all levels, which are estimated from the observations in Sect. 5 The linear response of Z500 is shown in Fig. 12a. The tripolar pattern of the observations shown in Fig. 2c is well reproduced.

This result supports the validity of the method of comparing the linear responses with the anomaly field.

Utilizing linearity of the model, we performed additional experiments investigating the effects of Q' and S' associated with convective activities separately from $\mathcal{N}$. The response to Q' and S' over the entire globe is shown in Fig. 12b. Three anomalies of positive–negative–positive appear from the Philippines to northeast of Japan. Although, the two anomalies in the low and midlatitudes are similar to that of the observations, the positive anomaly in the high latitudes is weak and shifted southeastward like Rossby wave propagation. In contrast, the response to $\mathcal{N}$, shown in Fig. 12c, has a clear positive anomaly around East Siberia similar to the observations. Therefore, the nonlinear forcings are important for the location and amplitude of the anomaly over East Siberia.

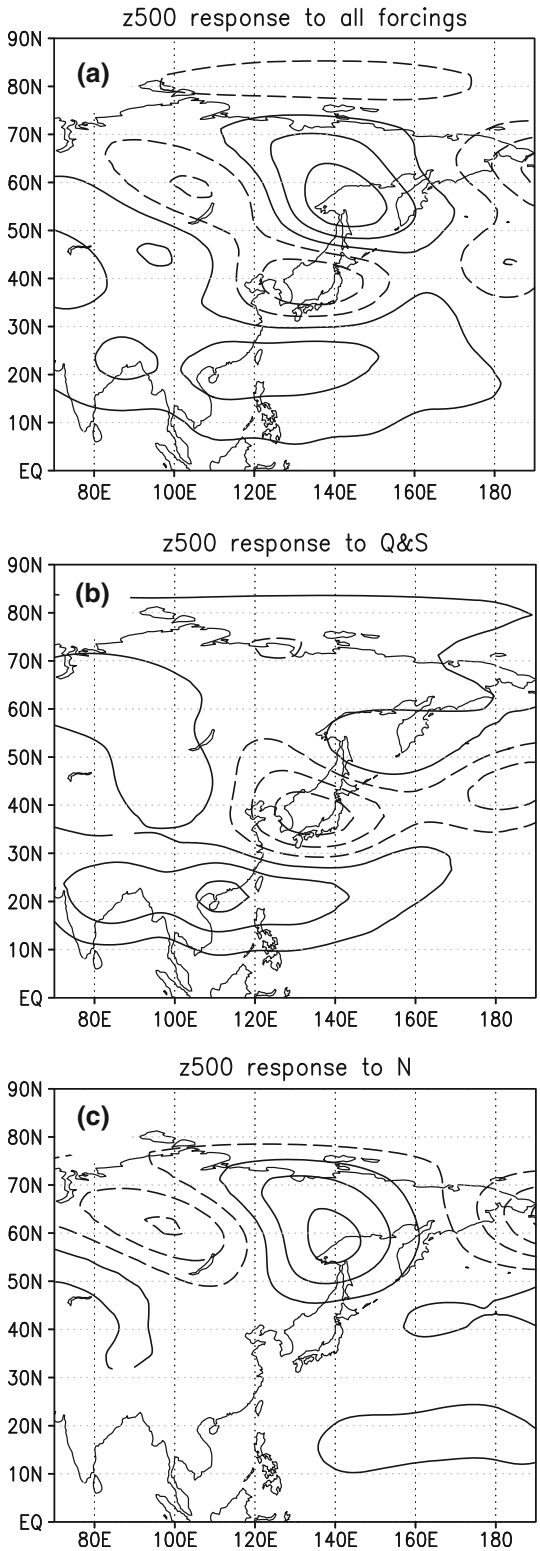

Fig. 12 Same as Fig. 2c, but Z500 of linear responses to **a** all forcings, **b** diabatic heating Q', and **c** nonlinear terms $\mathcal{N}$

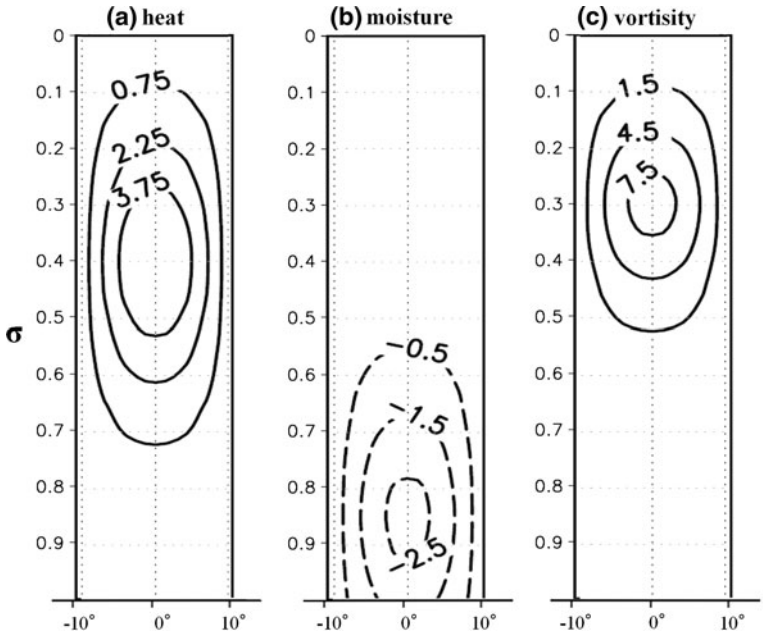

Fig. 13 Ideal forcings of **a** heat (K day^{-1}), **b** moisture (10^{-8} kg kg^{-1} s^{-1}), and **c** nonlinear vorticity flux (10^{-10} s^{-2})

5.1 The tripolar pattern as an internal mode

To examine whether internal processes are responsible for the formation of the pattern, we conducted a homogeneous forcing experiment similar to that conducted by Branstator (1990). We calculated a number of linear responses to external forcing distributed homogeneously over the Northern Hemisphere (indicated in Fig. 14a). Each forcing consisted of heating, moisture sink, and nonlinear vorticity forcing, as shown in Fig. 13. The amplitude and vertical structure of the forcings were determined on the basis of a global average of diabatic heating Q, moisture sink S, and a

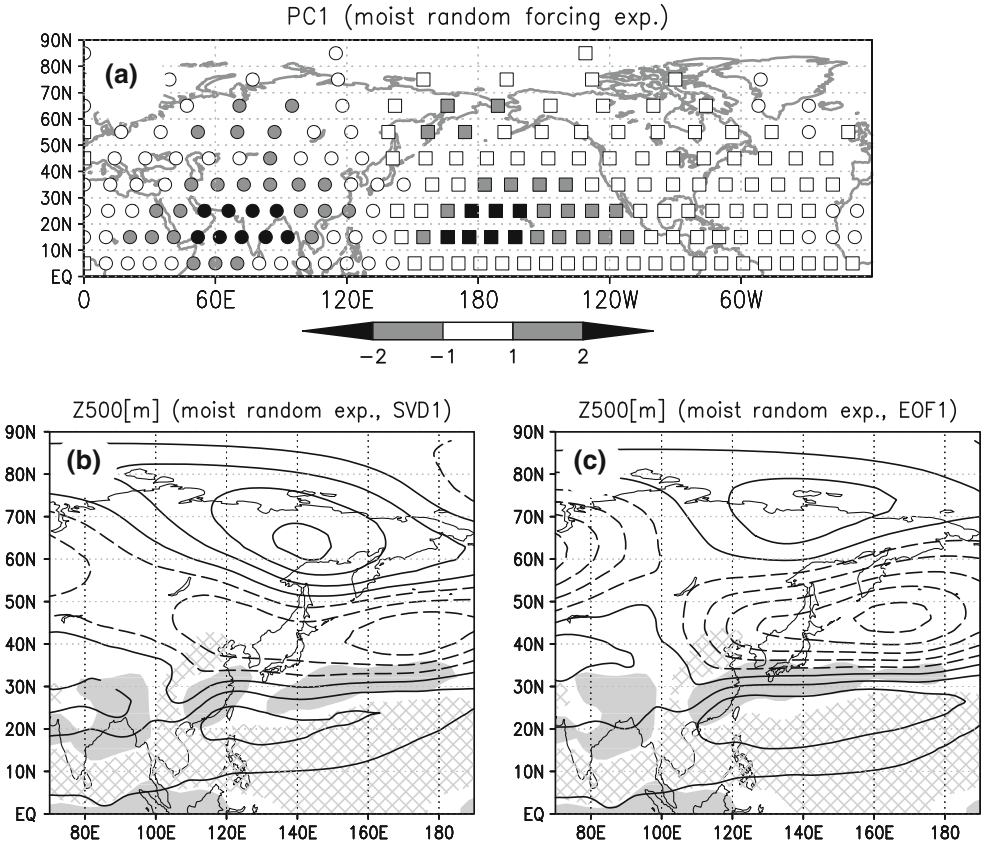

Fig. 14 A dominant response for a homogeneous forcing experiment. **a** Scores of a dominant response extracted as SVD1 (normalized by standard deviations). *Circles* and *squares* denote positive and negative values, respectively. **b** A regression map of precipitation (*hatchings* and *shadings*) and Z500 (*contours*) with respect to the scores of the SVD1. **c** The dominant pattern extracted as EOF1 is also shown for the comparison with Fig. 16. *Hatchings* and *shadings* in **b** and **c** show precipitation anomalies smaller than −0.2 mm day^{-1} and larger 0.2 mm day^{-1}, respectively. Contour an interval in **b** and **c** are 4 ($\pm 2, \pm 6, \pm 10, \ldots$) m

nonlinear term of the vorticity equation $\mathcal{N}_\xi$ estimated in the observations. After calculating all the responses over the Northern Hemisphere, we performed a SVD analysis of precipitation and Z500 over East Asia to these responses to obtain the dominant response. Because the forcing was homogeneously distributed, the structure of the dominant response is determined by internal processes rather than external forcing. Navarra (1993) showed that the dominant mode of a homogeneous forcing experiment corresponds to a Schmidt mode of the governing equations. Therefore, the dominant pattern extracted by this method can be considered an internal mode of the atmospheric system linearized about the basic state of the JJA climatology.

Figure 14 shows the dominant response derived as the SVD1 (SCF = 51 %) using the method described above. As in Fig. 2c, Z500 anomalies occur around the Philippines, China/Japan, and East Siberia. Therefore, the tripolar pattern can be referred to as a dominant pattern, even if the external forcing to the atmosphere is homogeneously distributed over the Northern Hemisphere. Figure 14a shows the scores of each response. Large positive (negative) values of circles (squares) indicate locations where forcing effectively excites the SVD1 (with opposite polarity). Scores greater than one standard deviation are located around India, the central Pacific, central Siberia, and east of Siberia. This multi-regional contribution is consistent with the idea of internal mode.

Figure 15 shows three examples of the linear responses. The linear response to forcing near India (62°E, 15°N; Fig. 15a) has the highest SVD score (2.94) of all the responses. A positive Z500 anomaly extends from India to the Philippines, whereas a positive–negative–positive wave train appears from Turkey to Siberia, and a negative anomaly is located around Japan. As in the observed SVD1

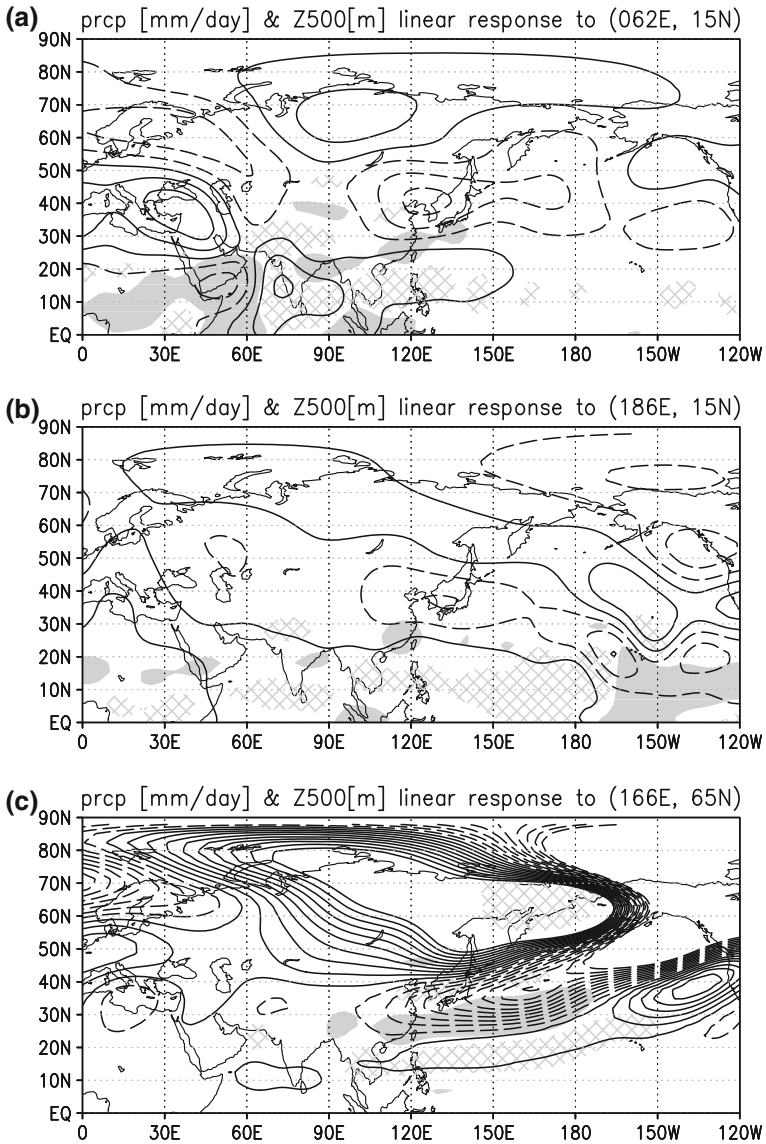

Fig. 15 Linear responses to the ideal forcings at **a** (62°E, 15°N), **b** (186°E, 15°N), and **c** (166°E, 65°N). *Hatchings* and *shadings* denote precipitation responses smaller than -1.8mm day^{-1} and larger than 1.8 mm day^{-1}, respectively. *Contours* show a Z500 response with an interval of 16 ($\pm 8, \pm 24, \pm 40, \ldots$) m. *Signs* in **b** and **c** are reversed corresponding to their negative SVD scores

in Sect. 3 (Fig. 2b) precipitation anomalies occur around the Philippines and China/Japan. The other two examples of the response to the forcing over the central Pacific (62°E, 15°N) and the East Siberia (166°E, 65°N) also show large contribution to the dominant pattern; their scores are −2.36 and −1.42, respectively. Note that the signs of the anomalies in Fig. 15b, c are reversed corresponding to their negative scores. Although all three responses have tripolar structure over the East Asia, their structures are very different over the other areas. These results further suggest the pattern is characterized by the internal processes in the East Asia and the external forcings play relatively minor roles.

The role of moist processes for the internal mode is examined by a similar homogeneous forcing experiment, but without moist processes. Precipitation cannot be defined (or is always zero) in such dry experiments. Therefore, the dominant pattern is extracted using the EOF analysis of Z500 over East Asia instead of the SVD analysis of precipitation and Z500. The EOF1 (explains 32 % of the total correlation) of the moist homogeneous experiment is shown in Fig. 14c for comparison.

The result of the dry homogeneous experiment is shown in Fig. 16. The dominant pattern extracted as the EOF1 (explains 23 %) shows three anomalies over East Asia. The large scores over Siberia and the northwest–southeast orientation of the three anomalies suggest the importance of the Rossby waves from the high latitudes in the upper troposphere in the dry experiment. These differences from the results of the moist experiment demonstrate the important role of the moist processes for the tripolar pattern.

The homogeneous forcing experiments are idealistic experiments and inconsistent with the real atmosphere in some parts. For example, in the real atmosphere, Q' and S' are concentrated over the low latitudes (Fig. 6c), whereas $\mathcal{N}$ is mostly identified in the mid and high latitudes (Fig. 8f). Some other homogeneous forcing experiments with different forcings are described in "Appendix 2".

5.2 Effects from the low and high latitudes

Additional experiments are carried out to investigate the relationships among the three anomalies. As described in Sect. 4, the Rossby waves in the lower and upper troposphere as well as the moist processes seem to be important for these relationships.

We conducted experiments calculating linear responses to the observed forcings Q', S', and $\mathcal{N}$ regionally confined around the Philippines (indicated by ① in Figs. 6c, d, 7f, and 8f). Figure 17 shows the results of moist and dry experiments. The Z500 (vorticity at 850 hPa) response in the moist experiment shows positive and negative (negative and positive) anomalies near the Philippines and Japan, respectively, and the WAF shows the northward Rossby waves from the Philippines, which are similar to that of the observations shown in Fig. 2 (Fig. 7a). Moreover, the

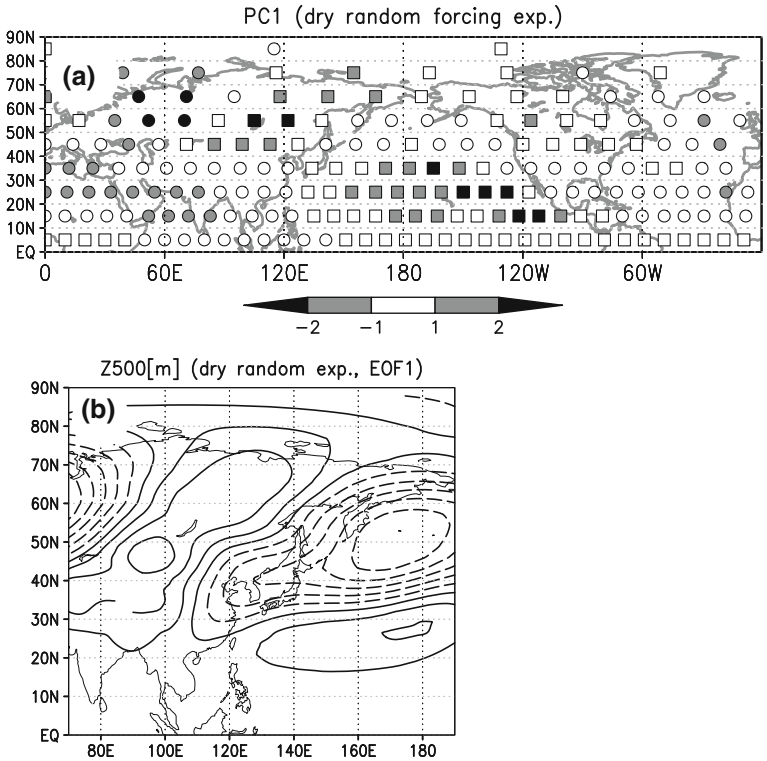

Fig. 16 Same as **a** Fig. 14a and **b** Fig. 14c, but for a homogeneous experiment without moist processes in which precipitation is not defined

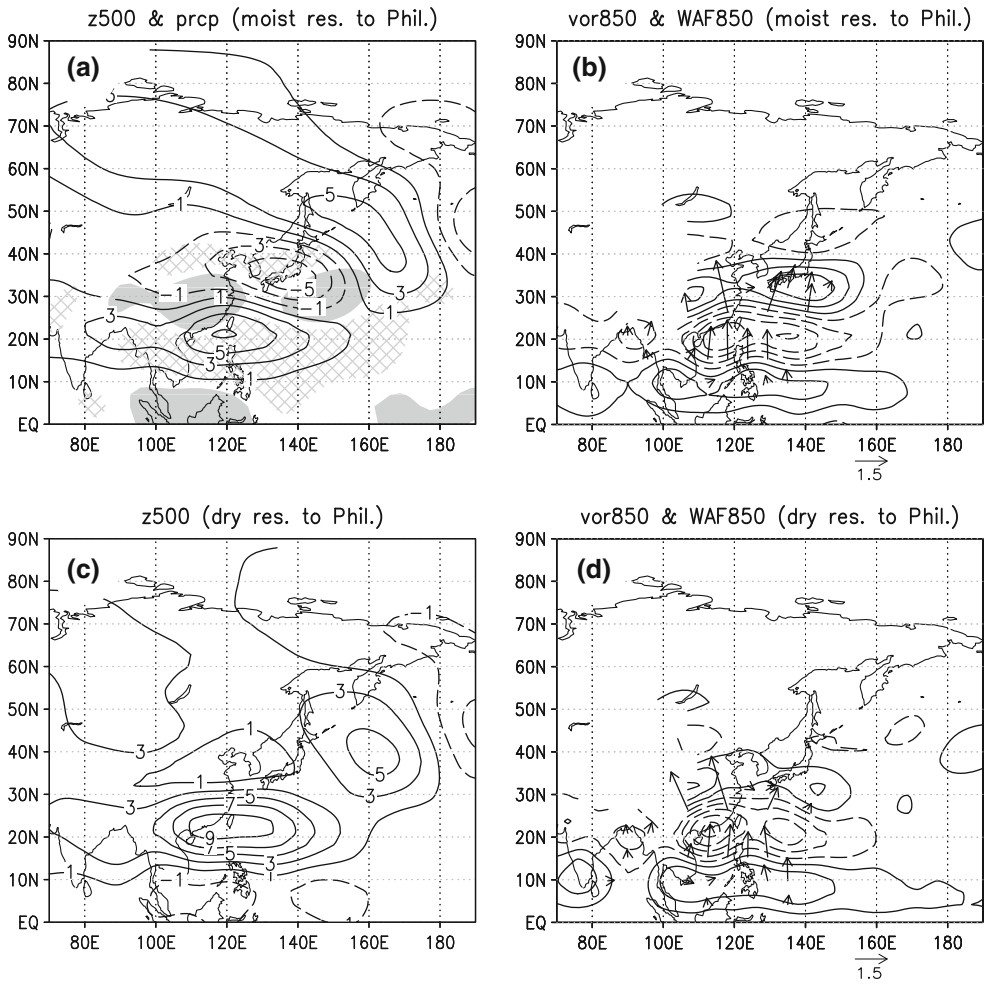

Fig. 17 Linear responses to the forcing around the Philippines in an experiment **a**, **b** with and **c**, **d** without moist processes. *Contours* in **a** and **c** indicate the Z500 response (m). *Hatchings* and *shadings* in **a** and **c** show precipitation responses smaller than -0.2 mm day^{-1} and larger 0.2 mm day^{-1}, respectively. *Contours* in **b** and **d** show vorticity response at 850 hPa with an interval of 12 ($\pm 6, \pm 18, \pm 30, \ldots$) $\times 10^{-6}$ s^{-1}, whereas vectors show WAF (m^{-2} s^{-2})

positive Z500 anomaly (negative vorticity anomaly) is identified to the north of Japan. On the other hand, in the dry experiment (Fig. 17c, d), vorticity anomalies appeared near the Philippines and China/Japan. However, the Z500 response around Japan is positive, and the vorticity anomaly to the north of Japan is not identified. This supports the importance of the Rossby waves and the moist processes discussed in Sect. 4.

The results of similar experiments with and without moist processes but the forcings confined around East Siberia (indicated by ②in Figs. 6c, d, 7f, and 8f) are shown in Fig. 18. In the moist experiment, negative–positive–negative vorticity anomalies and souteastward WAF are identified from East Siberia to southeast of Japan in the upper troposphere (Fig. 18a), which are similar to the observations shown in Fig. 8a. In the dry experiment, the negative anomaly over the southeast of Japan is shifted eastward and its zonally elongated structure is deformed (Fig. 18b), suggesting the importance of precipitation anomalies near Japan (Fig. 18a).

It is worth discussing the time evolutions of the moist responses. Figure 19 shows the vorticity response and the WAF on the 3rd day and the 7th day instead of a 15–20 day average shown in Fig. 17b. The vorticity responses around the Philippines and China/Japan appear immediately after the forcings are imposed. Then anomalies are gradually amplified, and the anomaly over the Sea of Othotsk appears around the 7th day. The steady state is obtained around the 15th day. Similarly, the time evolution of the response to the forcings around East Siberia indicates that the negative–positive–negative vorticity anomalies appear around the 7th day with the southeastward WAF, and the anomalies are amplified until the steady state shown in Fig. 18a is obtained around the 15th day.

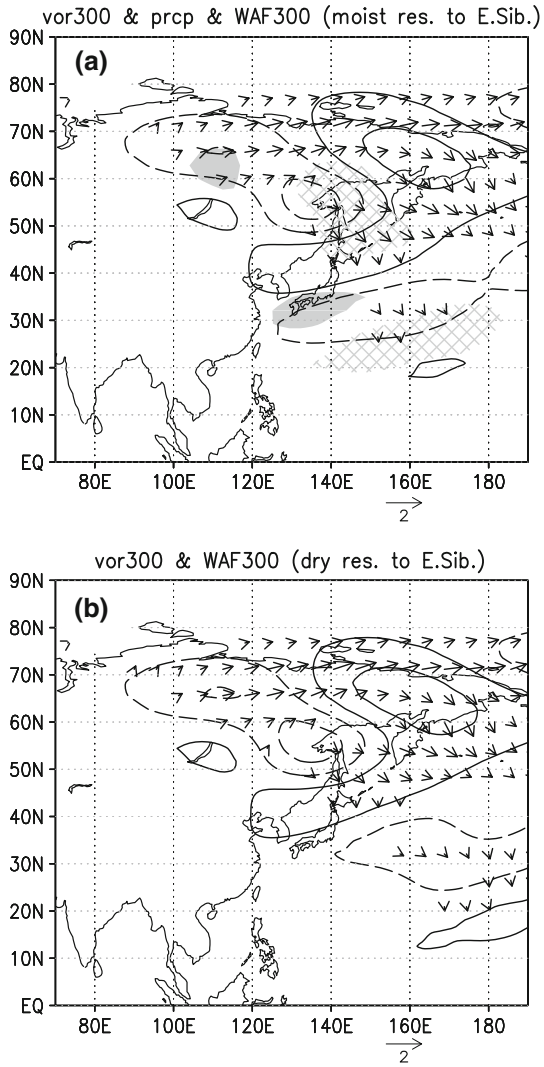

Fig. 18 Linear responses to the forcing around East Siberia in an experiment **a** with and **b** without moist processes. *Contours* in show vorticity response at 300 hPa with an interval of 16 $(\pm 8, \pm 24, \pm 40, \ldots) \times 10^{-6}$ s^{-1}, whereas vectors show WAF (m^{-2} s^{-2}). *Hatchings* and *shadings* in **a** show precipitation responses smaller than -0.2 mm day^{-1} and larger 0.2 mm day^{-1}, respectively

6 Summary and discussion

The SVD and EOF analyses demonstrate the importance of the tripolar pattern as a dominant pattern of EASM climate variability. Moreover, the results of the homogeneous forcing experiment suggest that the pattern remains a dominant, even if external forcing is homogeneously distributed over the Northern Hemisphere. In conclusion, the tripolar pattern can be thought of as an internal mode, characterized by the atmospheric internal processes.

In the pattern, the moist processes strengthen the circulation anomalies in the lower troposphere, the dynamical energy conversion supplies energy to the anomaly field from the climatological field, and the Rossby waves propagate northward in the lower troposphere and southeastward in the upper troposphere (Fig. 10). These processes are favorable for the pattern to have large amplitude and to influence a large area; thus, the pattern is dominant over the large area of East Asia or even the Northern Hemisphere (Fig. 3). These internal processes are closely related to the structure of the EASM climatological field, which is the reason for the location of the three anomalies.

In contrast with the PJ pattern, the processes in the higher latitudes are also involved in the tripolar pattern. The PJ pattern and the positive anomalies over East Siberia discussed separately in the previous studies are strongly related. It is interesting how the processes from the south and the north are related. The analysis of the omega equation in Sect. 3 and the response to the forcings around the Philippines (Fig. 17) suggest that the effects from the south reach farther to the north of Japan through the dynamically induced vertical velocity ω_D'. Present study also indicates that the moist processes of the rainband in the midlatitudes are important for the coupling of the south and the north. In fact, the tripolar structure of the homogeneous forcing experiment is deformed when the moist processes are removed (Fig. 16b). As the dry response to the forcings around the Philippines is not similar to the pattern (Fig. 17a), the effects from the lower latitudes do not contribute to the formation of the tripolar structure in the dry homogeneous experiments (Fig. 16a). The commitments of processes from the south and the north explain the south–north orientation of the three anomalies rather than the southwest–northeast orientation of simple Rossby waves.

In Sect. 5, we argued that the strong interactions of circulations and precipitation are identified over the low and midlatitudes of East Asia, but the causality is unclear from the diagnostic analyses. The model results in Sect. 2 show that the midlatitude precipitation can be triggered by remotely induced circulations from the tropics. The dry response to the forcings around the Philippines (Fig. 17d) shows low-level cyclonic anomaly in midlatitudes, and the moist response (Fig. 17a, b) suggests that the remotely induced convergence triggers precipitation in midlatitudes.

This study indicates the importance of the nonlinear processes (Fig. 8f) in the high latitudes (Fig. 12c). Further experiments separating the nonlinear terms $\mathcal{N}$ indicated that the effects shown in Fig. 12c are mainly due to the nonlinear terms of the vorticity equation $\mathcal{N}_\xi$, and other terms such as $\mathcal{N}_T$ have minor impacts (figures are not shown). However, we could not clarify how the nonlinear forcings $\mathcal{N}_\xi$ are determined. To answer this question, we need to understand how structures and frequency of subseasonal disturbances are different in the years of the positive and negative phase of the tripolar pattern. It is possible that the nonlinear effects are resulted as a response to the forcings in the lower latitudes. For example, a positive Z500 response

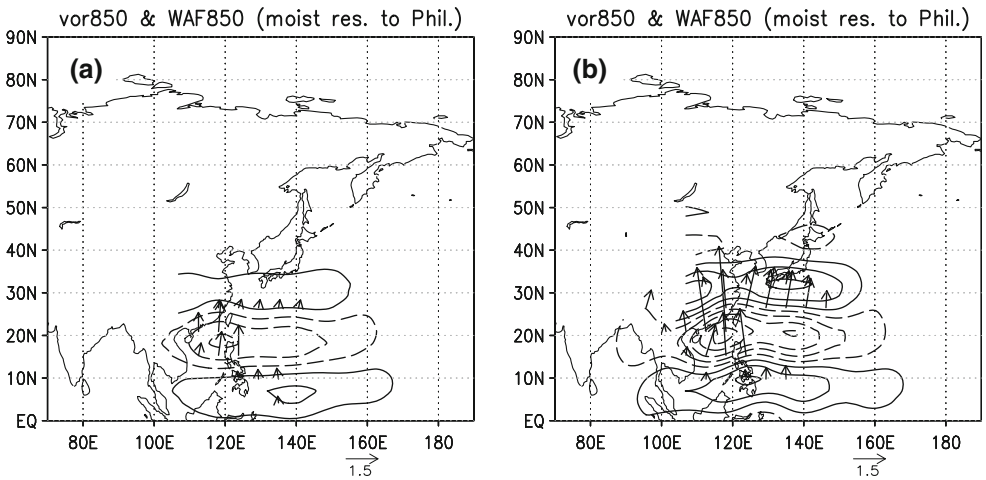

Fig. 19 Same as Fig. 17b, but for **a** the 3rd day and **b** the 7th day

to the forcings around the Philippines (Fig. 17a) appears in the high latitudes. Subseasonal disturbances and associated nonlinear effects will be affected by this response. Our model cannot reproduce these remotely-induced nonlinear effects. This lack may be a reason that the northernmost anomalies around East Siberia are not well reproduced. Understanding the nonlinear effects is an interesting issue that we will work in future.

As discussed in Sect. 3, the tripolar pattern is significantly correlated with the NINO3.4 SST and the Indian Ocean SST. Interestingly, the homogeneous forcing experiment suggests that India and the central Pacific are regions where the pattern can be effectively excited (Fig. 14a). Wang et al. (2000) and Xie et al. (2009) discussed how the SSTs over the NINO3.4 region and the Indian Ocean trigger circulation anomalies around the Philippines, respectively. Although this study focused on internal processes over East Asia, we will examine the mechanisms by which the tripolar pattern is excited in future.

Acknowledgments The authors appreciate Prof. Kimoto for the valuable suggestions. This work is supported by KAKENHI (24540469). JRA25/JCDAS reanalysis data are provided by the cooperative research project of the JRA25 long-term reanalysis by the Japan Meteorological Agency and the Central Research Institute of Electric Power Industry. CMAP Precipitation data is provided by the NOAA/OAR/ESRL PSD, Boulder, Colorado, USA, from their website at http://www.cdc.noaa.gov/. Figures were drawn by GrADS.

Appendix 1: SVD analyses for June, August, and daily data

The SVD analyses of precipitation and Z500 over East Asia (70°E–170°W, 0°–90°N) for June average data, August average data, and daily average data of 6/1–8/31 during 1979–2005[1] are performed (figures are not shown). All the Z500 anomaly fields of these SVD1s have the tripolar structure in common. The SCFs of the June and August SVD1 are both 46 %, and that of the daily data SVD1 is 30 %. These results indicate that the tripolar pattern is dominant from June to August. Moreover, the results of the daily data analysis suggest that the pattern is dominant also in the interseasonal variability.

There are some notable differences in the pattern of June–August. The anomalies around the Philippines and China/Japan in August seem to be shifted northward compared to that in June. The anomaly around East Siberia has a larger horizontal scale and is shifted relatively more westward in August than in June. These differences are probably related to the seasonal differences of a climatological mean field. For example, the rainband in the midlatitudes of a climatological field migrate northward from June to July, and its band structure disappears in August. The jet along the coastline of the Arctic Sea becomes weaker as the temperature over the Arctic Sea increases. It is interesting how they are related to the structure of the tripolar pattern, which is beyond the scope of this study.

Appendix 2: Sensitivities of the homogeneous forcing experiments

We performed two homogeneous forcing experiments in order to extract a dominant pattern for responses to the Q' and S' forcings over the low latitudes (0°–30°N) and a dominant pattern for the $\mathcal{N}_\xi$ over the mid and high latitudes (30°–90°N) (figures are not shown). The positive and

[1] Daily precipitation is interpolated from pentad CMAP precipitation data, which does not include variations with a period shorter than 5 days. Similar results are obtained even when daily precipitation from the JRA reanalysis is used.

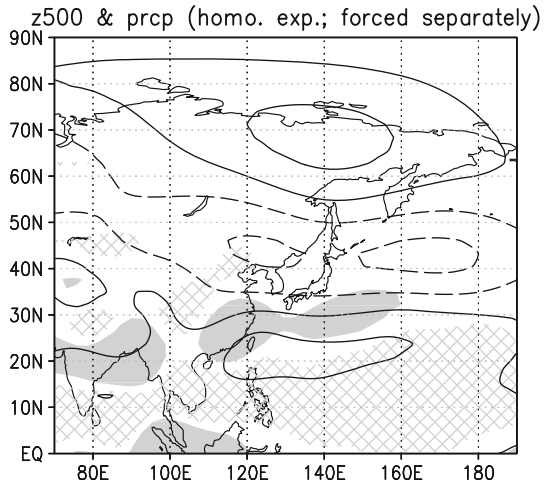

Fig. 20 Same as Fig. 14b, but a dominant response of a homogeneous forcing experiment for forcings Q'/S' and $\mathcal{N}_\xi$ prescribed separately over the Northern Hemisphere

negative anomalies appeared around the Philippines and Japan, respectively, in the SVD1 (24 %) for the Q' and S' in the low latitudes. On the other hand, the anomalies of the mid and high latitudes are emphasized in the SVD1 (37 %) for the $\mathcal{N}_\xi$ over the mid and high latitudes.

We performed another homogeneous forcing experiment with Q'/S' and $\mathcal{N}_\xi$ prescribed separately before SVD analyses are conducted. The dominant response obtained from this experiment is shown in Fig. 20. The dominant response (SVD1; 61 %) has almost the same tripolar structure as that of the experiment with forcings prescribed together (Fig. 14b).

References

Arai M, Kimoto M (2008) Simulated interannual variation in summertime atmospheric circulation associated with the East Asian monsoon. Clim Dyn 31:435–447

Branstator G (1990) Low-frequency patterns induced by stationary waves. J Atmos Sci 47:629–648

Endo H (2005) An analysis of a cool summer in 2003. Meteorol Study Note 210:99–110 (in Japanese)

Enomoto T, Hoskins BJ, Matsuda Y (2003) The formation mechanism of the Bonin high in August. Q J R Meteorol Soc 587:157–178

Fukutomi Y, Yasunari T (1999) 10–25 day intraseasonal variations of convection and circulation over East Asia and western North Pacific during early summer. J Meteorol Soc Jpn 77:753–769

Fukutomi Y, Yasunari T (2002) Tropical-extratropical interaction associated with the 10–25-day oscillation over the western pacific during the northern summer. J Meteorol Soc Jpn 80:311–331

Hirota N, Takahashi M, Sato N, Kimoto M (2005) Recent climate trends in the East Asia during the Baiu season of 1979–2003. SOLA 1:137–140

Kimoto M (2005) Simulated change of the east Asian circulation under global warming scenario. Geophys Res Lett 32:L16701

Kosaka Y, Nakamura H (2006) Structure and dynamics of the summertime Pacific–Japan teleconnection pattern. Q J R Meteorol Soc 132:2009–2030

Kosaka Y, Nakamura H (2008) A comparative study on the dynamics of the Pacific–Japan (PJ) teleconnection pattern based on reanalysis datasets. SOLA 4:9–12

Kosaka Y, Nakamura H (2010) Mechanisms of meridional teleconnection observed between a summer monsoon system and a subtropical anticyclone. Part I: the Pacific–Japan pattern. J Clim 23:5085–5108

Lu R, Lin Z (2009) Role of subtropical precipitation anomalies in maintaining the summertime meridional teleconnection over the western North Pacific and East Asia. J Clim 22:2058–2072

Navarra A (1993) A new set of orthonormal modes for linearized meteorological problems. J Atmos Sci 50:2569–2583

Ninomiya K, Mizuno H (1985) Anomalous cold spell in summer over northeastern Japan caused by northeasterly wind from polar maritime air-mass. Part I: EOF analysis of temperature variation in relation to the largescale situation causing the cold summer. J Meteorol Soc Jpn 63:845–857

Nitta T (1987) Convective activities in the tropical western Pacific and their impact on the northern hemisphere summer circulation. J Meteorol Soc Jpn 65:373–390

North G, Bell T, Cahalan R, Moeng F (1982) Sampling errors in the estimation of empirical orthogonal functions. Mon Weather Rev 110:699–706

Numaguti A, Takahashi M, Nakajirna T, Sumi A (1995) Development of an atmospheric general circulation model. In: Climate system dynamics and modelling. Center for Climate System Research, University of Tokyo, Tokyo, pp 1–27

Onogi K et al (2007) The JRA-25. J Meteorol Soc Jpn 85:369–432

Sato N, Takahashi M (2007) Dynamical processes related to the appearance of the Okhotsk high during early midsummer. J Clim 20:4982–4994

Satoh M (2004) Atmospheric circulation dynamics and general circulation models. Springer/PRAXIS, ISBN: 3-540-42638-8

Simmons AJ, Wallace JM, Blanstator GW (1983) Barotropic wave propagation and instability, and atmospheric teleconnection patterns. J Atmos Sci 40:1363–1392

Takaya K, Nakamura H (2001) A formulation of a phase independent wave-activity flux for stationary and migratory quasigeostrophic eddies on a zonally varying basic flow. J Atmos Sci 58:608–627

Tsuyuki T, Kurihara K (1989) Impact of connvective activity in the Western Tropical Pacific on the East Asian summer circulation. J Meteorol Soc Jpn 67:231–247

Wallace JM, Gutzler DS (1981) Teleconnections in the geopotential height field during the Northern Hemisphere winter. Mon Weather Rev 109:784–812

Wang B, Wu R, Fu X (2000) Pacific–East Asian teleconnection: how does ENSO affect East Asian climate? J Clim 13:1517–1536

Wang B, Wu R, Lau K-M (2001) Interannual variability of Asian summer monsoon: contrasts between the Indian and the Western North Pacific–East Asian Monsoons. J Clim 14:4073–4090

Watanabe M, JIN F (2003) A moist linear baroclinic model: coupled dynamical-convective response to El Nino. J Clim 16:1121–1139

Watanabe M, Kimoto M (2000) Atmosphere–ocean thermal coupling in the North Atlantic: a positive feedback. Q J R Meteorol Soc 126:3343–3369

Watanabe M, Kimoto M (2001) Corrigendum. Q J R Meteorol Soc 127:733–734

Xie P, Arkin PA (1997) Global precipitiation: a 17 year monthly analysis based on gauge observations, satellite estimates, and numerical model outputs. Bull Am Meteorol Soc 78:2539–2588

Xie S-P, Hu K, Hafner J, Tokinaga H, Du Y, Huang G, Sampe T (2009) Indian ocean capacitor effect on Indo-western Pacific climate during the summer following El Nino. J Clim 22:730–747

Yanai M, Esbensen S, Chu J-H (1973) Determination of bulk properties of tropical cloud clusters from large-scale heat and moisture budgets. J Atmos Sci 30:611–627

Yasutomi N (2003) Detection and dynamics of principal modes of Asian summer monsoon variability. PhD thesis, University of Tokyo, Department of Earth and Planetary Science, Graduate School of Science